Published in final edited form as:
Biochemistry. 2008 May 27; 47(21): 5869–5880.

Shotgun Lipidomics Reveals the Temporally Dependent, Highly Diversified Cardiolipin Profile in the Mammalian Brain: Temporally Coordinated Postnatal Diversification of Cardiolipin Molecular Species with Neuronal Remodeling†

Hua Cheng, **David J. Mancuso**, **Xuntian Jiang**, **Shaoping Guan**, **Jingyue Yang**, **Kui Yang**, **Gang Sun**, **Richard W. Gross**, and **Xianlin Han***
Division of Bioorganic Chemistry and Molecular Pharmacology, Department of Internal Medicine, Washington University School of Medicine, St. Louis, Missouri 63110

Abstract

Large-scale neuronal remodeling through apoptosis occurs shortly after birth in all known mammalian species. Apoptosis, in large part, depends upon critical interactions between mitochondrial membranes and cytochrome *c*. Herein, we examined the hypothesis that the large-scale reorganization of neuronal circuitry after birth is accompanied by profound alterations in cardiolipin (CL) content and molecular species distribution. During embryonic development, over 100 CL molecular species were identified and quantitated in murine neuronal tissues. The embryonic CL profile was notable for the presence of abundant amounts of relatively short aliphatic chains (e.g., palmitoleic and oleic acids). In sharp contrast, after birth, the CL profile contained a remarkably complex repertoire of CL molecular species, in which the signaling fatty acids (i.e., arachidonic and docosahexaenoic acids) were markedly increased. These results identify the rapid remodeling of CL in the perinatal period with resultant alterations in the physical properties of the mitochondrial membrane. The complex distribution of aliphatic chains in the neuronal CL pool is separate and distinct from that in other organs (e.g., heart, liver, etc.), where CL molecular species contain predominantly only one major type of aliphatic chain (e.g., linoleic acid). Analyses of mRNA levels by real-time quantitative polymerase chain reactions suggested that the alterations in CL content were due to the combined effects of both attenuation of *de novo* CL biosynthesis and decreased remodeling of CL. Collectively, these results provide a new perspective on the complexity of CL in neuronal signaling, mitochondrial bioenergetics, and apoptosis.

Cardiolipin (1,3-diphosphatidyl-*sn*-glycerol, CL)[1]is exclusively present in the mitochondrial membrane of eukaryotic cells (1), whose evolutionary origins can be traced back to bacterial membranes. Each CL molecular species is uniquely comprised of a dimer of two phosphatidyl

†This work was supported by NIA Grants R01 AG23168 and R01 AG31675, NIH Grant P01 HL57278, and the Neurosciences Education and Research Foundation.

* To whom correspondence should be addressed: Division of Bioorganic Chemistry and Molecular Pharmacology, Department of Internal Medicine, Washington University School of Medicine, Box 8020, 660 South Euclid Avenue, St. Louis, MO 63110. Telephone: (314) 362−2690. Fax: (314) 362−1402. E-mail: xianlin@wustl.edu..

[1]Abbreviation: CL, cardiolipin; FA, fatty acid or fatty acyl; FACO, fatty acyl-CoA oxidase; GAPDH, glyceraldehyde-3-phosphate dehydrogenase; HPLC, high-performance liquid chromatography; iPLA2β and γ, calcium-independent phospholipase A2β and γ, respectively; *m*:*n*, acyl chain containing *m* carbons and *n* double bonds; RT–PCR, reverse transcription–polymerase chain reaction.

moieties (containing a total of four fatty acyl chains) connected by a molecule of glycerol. A chiral center is potentially present in each of the three glycerol moieties. This special structure of CL results in many unique physical and chemical properties, including a high negatively charged density, a large ratio of total fatty acyl chain/headgroup volume, an intricate configurational regiospecificity, and a specific affinity for cytochrome *c*. These unique properties, in turn, promote its role as an effector of many highly specific biological functions through specific interactions with multiple mitochondrial proteins (1–3). Several lines of evidence support a direct relationship between CL loss (or changes in CL molecular species) and cytochrome *c* release as an initial step in the pathway to apoptosis (4–8).

Thousands of distinct molecular species (calculated as N^4, where N is the number of fatty acid species found in CL) can theoretically be present in cellular membranes if all naturally occurring fatty acids were randomly incorporated into CL (9). Although this is true to some extent, biological organisms contain predominantly only one fatty acyl species (linoleic, 18:2 FA in most cases) with a minimal amount of other fatty acids for CL in normal tissues to achieve a maximal symmetric pattern of CL molecular species. For example, approximately 80 mol % of the fatty acyl (FA) moieties of CL molecular species in wild-type mouse heart, liver, and muscle are predominantly comprised of 18:2 FA (10). This selective incorporation of FA results in almost equal amounts (40 mol %) of configurationally symmetric (e.g., T18:2 CL) and quasi-symmetric CL molecular species (i.e., those containing one other FA besides 18:2 FA, such as 18:2−18:2−18:2−18:1 CL) in these organs (10). This specificity is achieved through the coordinated biosynthetic (e.g., phosphatidylglycerol phosphate synthase and CL synthase) and remodeling [e.g., phospholipases and transacylation/acyltransferation enzymes (e.g., tafazzins)] pathways (11–13).

It has been proposed that maximal CL molecular symmetry is necessary for tight interactions of CL with mitochondrial proteins (9). Therefore, any physiological and pathological perturbation in CL synthetic and/or catabolic pathways affects mitochondrial structure and function and ultimately cell survival. This essential role of CL in mitochondrial function has been underscored through identification of a genetic disorder, Barth syndrome, in which mutations in an X-linked gene, tafazzin, induce an altered CL metabolism, precipitate mitochondrial dysfunction and result in a striking cardiomyopathy (14,15). It has recently been demonstrated that altered CL content or composition is present in hypertensive rats undergoing heart failure (16,17) and may be related to Parkinson's disease (18) as well as traumatic brain injury (19). Substantially altered CL content and molecular composition in the heart occur at the very early stages of diabetes and are associated with mitochondrial dysfunction (20). We have demonstrated that the altered CL profile in diabetic myocardium results, in large part, from the activation of phospholipases in diabetic myocardium (21).

Active neuronal remodeling accomplished in large part through massive amounts of programmed cell death in the cortex in the perinatal period has been previously well-documented (22,23). Central to the apoptotic process is the release of cytochrome *c* from the inner mitochondrial membrane to the cytosol, where it can activate cytosolic caspases that initiate a “programmed” response, leading to highly structured and temporally coordinated cell death (23). Because cytochrome *c* binds to CL and its release is a central part of apoptosis, it is logical to consider the potential role of alterations in CL content and/or molecular composition that occur during the transition from the embryonic to the adult brain. In this study, employing a newly developed, enhanced shotgun lipidomics approach (10), we demonstrated the presence of changes in the CL molecular species profile in the perinatal period that is temporally correlated to the massive alterations in neuronal remodeling and apoptosis that occur after birth. Through exploiting the power of enhanced shotgun lipidomics, we identified the marked CL remodeling and the unanticipated diversity of brain CL molecular species in the perinatal period that could potentially serve multiple signaling functions.

MATERIALS AND METHODS

Materials

Synthetic 1,1′,2,2′-tetramyristoyl CL (T14:0 CL) was purchased from Avanti Polar Lipids, Inc. (Alabaster, AL) and quantitated by capillary gas chromatography prior to being used as an internal standard. Solvents for sample preparation and mass spectrometric analysis were obtained from Burdick and Jackson (Honeywell International, Inc., Burdick and Jackson, Muskegon, MI). All cell culture medium and reagents, unless mentioned specifically, were purchased from Gibco-Invitrogen (Grand Island, NY). All other chemical reagents were at least analytical-grade or the best grade available and obtained from either Thermo-Fisher Scientific (Pittsburgh, PA) or Sigma-Aldrich Chemical Co. (St. Louis, MO) or as indicated.

Preparation of Lipid Extracts from Biological Samples

Human postmortem brain samples from cognitively normal individuals at 80 ± 4 years of age were obtained from the brain bank of the Washington University ADRC Neuropathology/ Tissue Resource Core. Male New Zealand white rabbits (2−3 lbs. body weight) were purchased from Myrtles Rabbitry, Inc. (Thompson Station, TN). Male Sprague–Dawley rats (226−250 g body weight, approximately 2 months of age) were purchased from Charles River Laboratories, Inc. (Wilmington, MA). Mice with mixed gender on a C57BL/6 background at the indicated ages, as well as pregnant mice were purchased from The Jackson Laboratory (Bar Harbor, ME). Aged C57BL/6 mice were obtained from supplementation of the National Institute on Aging. When necessary, mice were housed in a full barrier facility with a 12 h light/dark cycle and maintained on standard chow (Diet 5053; Purina, Inc., St. Louis, MO).

Animals were sacrificed by asphyxiation with carbon dioxide. All animal procedures were performed in accordance with the “Guide for the Care and Use of Laboratory Animals” (National Academy of Science, 1996) and were approved by the “Animals Studies Committee” at Washington University. Brain tissues were dissected and immediately freeze-clamped at the temperature of liquid nitrogen. Wafers were pulverized into a fine powder with a stainless-steel mortar and pestle. Protein assays on the fine powders were performed using a bicinchoninic acid–protein assay kit (Pierce, Rockford, IL) with bovine serum albumin as a standard.

Fine powders of individual tissue sample (approximately 10 mg) were weighed in a disposable glass culture test tube. An internal standard, i.e., T14:0 CL (1.33 nmol/mg of protein), was added to each brain tissue homogenate based on the protein concentration, thereby allowing the final quantified lipid content to be normalized to the protein content and eliminate variabilities between the samples. Lipids from each homogenate were extracted by a modified Bligh and Dyer procedure (24) as described previously (25). Each lipid extract was reconstituted with a volume of 500 μL/mg of protein (on the basis of the original protein content of the samples as determined from protein assays) in chloroform/methanol (1:1, v/v). The lipid extracts were flushed with nitrogen, capped, and stored at −20 °C for electrospray ionization mass spectrometric analyses (typically within 1 week). Each lipid solution was diluted approximately 100-fold immediately prior to infusion and lipid analysis.

Instrumentation and Mass Spectrometry

High-resolution-based shotgun lipidomics analyses of CL were performed on either a quadrupole-time-of-flight (QqTOF) hybrid mass spectrometer (Applied Biosystems/MDS Sciex QStar XL, Concord, Canada) or a triple-stage quadrupole (QqQ) mass spectrometer (Thermo Scientific, San Jose, CA), both equipped with an ionspray ion source as previously described (10). Analyses of individual molecular species in other lipid classes were not performed in the study. However, some quantitative data can be found in our previous studies

(25). All electrospray ionization mass spectrometric analyses of lipids were conducted by direct infusion, employing a Harvard syringe pump at a flow rate of 4 μL/min. Typically, a 1 min period of signal averaging was employed for each mass spectrum, and a 2 min period of signal averaging was employed for each tandem mass spectrum. For product ion analyses by the QqTOF mass spectrometer, the precursor ion was selected by the first quadrupole, with a mass window of 0.7 Thomson. A mass resolution of 0.4 Thomson was employed for acquisition of mass spectra with the QqQ instrument.

Isolation and Culture of Mouse Embryonic Cortical Neurons

Primary neuron cultures were prepared as described previously (26). Briefly, mice (C57BL/6) at 15−17 days gestation were anesthetized, and the brains of embryos were removed. Dissociated neocortices were plated onto 6- or 24-well culture plates (Falcon, Franklin Lakes, NJ) at a density of ~4−7 hemispheres per plate that had been precoated with ploy-D-lysine (100 μg/mL) and laminin (5 μg/mL) prior to plating. Cells were grown in Dulbecco's minimum Eagle's medium supplemented with 20 mM glucose (or as indicated), 26 mM sodium bicarbonate, 2 mM L-glutamine, 5% fetal bovine serum and/or 5% horse serum (Hyclone, Logan, UT) or as indicated, 1 × Pen/Strep, and 1 × Fungizone for either 7 or 15 days. Cytosine arabinoside (10 μM) was added ~2−3 days after plating to halt the growth of non-neuronal cells.

Real-Time Reverse Transcription–Polymerase Chain Reaction (RT-PCR) Analyses of CL Biosynthesis and Remodeling Enzyme Message Levels

Total RNA was isolated with an RNeasy tissue kit and reverse transcribed with TaqMan reverse transcription reagents (Applied Biosystems, Foster City, CA). Quantitative PCR reactions were performed in triplicate in a 96-well format using TaqMan core reagents and a Prism 7700 Sequence Detector (Applied Biosystems, Foster City, CA) as previously described (21). The mouse-specific primer-probe sets used to detect specific gene expression included CL synthase (5′-TCGCTGCTGTGTTTTATGTCAGA/5′-TGGCATAGCAAGGATTGAAGTACT/5′-TCTGCCAACACCGCGAACACTAGC), calcium-independent phospholipase $A_2\beta$ (iPLA$_2\beta$) (5′-CCTTCCATTACGCTGTGCAA/5′-GAGTCAGCCCTTGGTTGTT/5′-CCAGGTGCTACAGCTCCTAGGAAAGAATGC), iPLA$_2\gamma$ (5′-GAGGAGAAAAAGCGTGTGTTACTTC/5′-GGTTGTTCTTCTTAAGGCCTGAA/5′-TCTGTTATCAATACTCACTCTTGCAATA), tafazzin (5′-GATCCTAAAACTCCGCCACATC/5′-GCAGCTCCTTGGTGAAGCA/5′-CTGCTGGGGTCCAACGCATCAACTT), and fatty acyl-CoA oxidase (FACO) (5′-GGATGGTAGTCCGGAGAACA/5′-AGTCTGGATCGTTCAGAATCAAG/5′-TCTCGATTTCTCGACGGCGCCG). Rodent GAPDH primers (Applied Biosystems, Foster City, CA) were used within the same well for normalization of gene expression.

Chemical Synthesis of T22:6 CL

Chemical synthesis of T22:6 CL was achieved through modification of a published approach (27). Briefly, *O*-chlorophenyl- and tetrahydropyranyl-protected T22:6 CL was prepared in a single reaction via phosphorylation of di22:6 glycerol in the presence of 2-*O*-tetrahydropyranylpropanol and subsequently phosphorylated using the bifunctional phosphorylating reagent, *O*-chlorophenyl dichlorophosphate. Sequential deprotection of *O*-chlorophenyl- and tetrahydropyranyl-protecting groups yielded T22:6 CL, which was purified by normal-phase high-performance liquid chromatography (HPLC) before use (28).

Preparation of Mouse Brain and Heart Mitochondria and Determination of the Rate of Mitochondrial Fatty Acid β-Oxidation

Brain and myocardial mitochondria of mice at 4 months of age were isolated as previously described (29,30) with minor modifications. Briefly, harvested organs were separately minced and homogenized on ice with 10% (wt/vol) of an isotonic isolation buffer containing 20 mM *N*-2-hydroxyethylpiperazine-*N*′-2-ethanesulfonic acid (HEPES) (pH 7.4), 140 mM KCl, 10 mM ethylenediaminetetraacetic acid (EDTA), and 5 mM $MgCl_2$ supplemented with protease inhibitors. The homogenate was centrifuged at 500*g* for 10 min. The cellular debris, nuclei, and connective tissue were discarded, and the supernatant was centrifuged at 9000*g* for 35 min. The pellet was then washed with the isolation buffer without protease inhibitors and resuspended in 80 μL of isolation buffer. The isolated mitochondria were characterized by determination of the respiratory control ratio as previously described (31). The rates of mitochondrial fatty acid β-oxidation were determined using a modified procedure as described (32). Briefly, respiration buffer containing 1-[^{14}C]-palmitic acid (150 μM) and fatty acid-free bovine serum albumin (3.5 mg/mL) was placed in a large scintillation vial, and the mixture was incubated at 35 °C for 20 min under a flow of 95% O_2/5% CO_2 gas. Isolated mitochondria (~30 mg of protein/mL) were added to the respiration solution with gentle shaking to give final mitochondrial protein concentrations of 5 and 0.7 mg/mL from the brain and heart, respectively. An Eppendorf tube (cap removed) containing 0.2 mL of 1 M benzethonium hydroxide was placed in each reaction vial, which was then quickly sealed and allowed to incubate at 35 °C for 30 min with shaking. The reactions were stopped by injection of 0.3 mL of concentrated HCl, and the sealed vials were incubated at room temperature overnight. The Eppendorf tube in each reaction vial was transferred to a scintillation vial, and the radioactivity of the trapped $^{14}CO_2$ was quantified by scintillation spectrometry.

Data Processing and Analyses

Data processing from the shotgun lipidomics analyses (including ion peak selection, baseline correction, data transferring, ^{13}C-de-isotoping, peak intensity comparisons, and content calculations) was conducted using a customized program based on Microsoft Excel macros developed as outlined previously (33). Data from biological samples were normalized to the protein content for lipid analyses. All data are presented as the mean ± SD of $n \geq 4$ for lipid analyses and $n \geq 3$ for quantitative RT-PCR analyses. Statistical differences between mean values were determined by nested analysis of variation (ANOVA) analysis.

RESULTS

Diversified Profile of CL Molecular Species Is Present in the Lipid Extracts of Mouse Brain Samples

Previous studies have shown that linoleic acid (18:2 FA) is the predominant fatty acyl chain (>75 mol %) in CL molecular species in almost all examined organs, tissues, and cells (10). The results in previously examined tissues identify CL species containing either three or four 18:2 FA chains as the predominant molecular species in CL from heart, skeletal muscle, and liver. In sharp contrast, enhanced shotgun lipidomics analyses of the lipid extracts of mouse cortex demonstrated a distinct profile comprised of diverse CL molecular species (Figure 1A). Specifically, the profile of cortex CL molecular species was observed through a broad mass range (Figure 1A), and the relative abundance of the majority of these CL molecular species was comparable (see the distribution of the asterisks in Figure 1A). Further analyses showed that over 100 distinct CL molecular species (not including regioisomers) were readily identified (Table 1).

To determine whether our recently developed enhanced shotgun lipidomics methodology allowed us to accurately quantitate the content of CL molecular species over a broader mass

range than that which we have examined previously (10), we synthesized T22:6 CL and purified it by HPLC as described under the Materials and Methods. This purified material was used to generate a standard curve to compare ionization efficiency to the traditionally used commercially available standard for CL (i.e., T14:0 CL) (Figure 2). The results demonstrated that CL molecular species could be quantitated over a very broad mass range, with results similar to those obtained employing the traditionally used T14:0 CL internal standard after ^{13}C de-isotoping of each individual molecular species (parts B and C of Figure 2).

Therefore, the enhanced shotgun lipidomics approach was employed to determine the content of CL molecular species of mouse cortex and other brain regions. Analysis of the individual molecular species content of mouse cortex CL molecular species demonstrated a broad range of fatty acyl chain composition. The composition of fatty acyl chains in the cortex CL pool was (mol % in parentheses) 18:1 (41), 20:4 (24), 22:6 (13), 18:2 (9), 16:1 (6), 16:0 (4), and 18:0 (1) FA for mice at 4 months of age (Table 1).

In addition to the CL molecular species in the cortex, shotgun lipidomics analyses demonstrated the diversified CL profiles in other examined brain regions, including brain stem, cerebellum, and spinal cord (Figure 1B and Table 1). The total CL contents of most of these functionally distinct regions were essentially identical (Table 1). However, the compositions of 18:1 FA in the CL pools of the brain stem and spinal cord are relatively higher than those in cortex and cerebellum (Table 1). This difference in 18:1 FA composition may represent the influence of endogenous fatty acids (acyl-CoAs) because our previous studies have demonstrated that the major phospholipid pools in white matter contain predominantly 18:1 fatty acids in contrast to the enrichment of polyunsaturated fatty acids in gray matter phospholipids (34).

Brain CL Molecular Species Diversity Was Present among All Examined Mammalian Species

Next, studies were performed to examine whether the diversified CL molecular species profile was specific to mouse brain. We compared the CL content and individual molecular species composition of lipid extracts from human, rabbit, and rat brain to those present in mouse to determine if species-specific variations were present. Shotgun lipidomics analysis demonstrated that a diversified profile of CL molecular species was consistently present in all examined brain samples. However, we point out that specific variations in CL molecular species composition were present in different mammalian species (Figure 3, compared to Figure 1). The effects of age on the diversity of the brain CL profile of the mammals were determined to be minimal as documented below.

Diversity of CL Molecular Species in Mouse Cortex Is Highly Dynamic during Development but Remains Constant after Maturation

Next, enhanced shotgun lipidomics revealed that the total CL levels in mouse cortex significantly increased during development *in utero*, transiently decreased at birth (i.e., day 0, inset of Figure 4A), and then began to increase in the postnatal period. Intriguingly, marked alterations in the levels of individual CL molecular species (Figure 4B) and the composition of the FA chains in the CL pool (Figure 5) were manifest in the perinatal period. For example, the content of di16:1–di18:1 CL (i.e., *m*/*z* 699.5) decreased from 0.78 (day −7) to 0.04 nmol/mg of protein (day 20) (Figure 4B). The content of 16:1−18:1−18:1−18: 1/16:0−18:1−18:1 −18:2 CL (i.e., *m*/*z* 713.5) decreased from 0.60 (day −7) to 0.18 nmol/mg of protein (day 20) (Figure 4B).

Moreover, 18:1 and 16:1 FA were the predominant molecular species in mouse cortical CL molecular species at 7 days before birth, accounting for 37 and 26 mol %, respectively (Figure 5A). During the development of the brain, the content of CL 18:1 FA decreased to a minimum at day 7 after birth (Figure 5A) before gradually increasing through day 60. In contrast, the

level of 16:1 FA was markedly reduced from 26 to 10 mol % during this period. The content of 20:4 FA in the CL pool increased approximately 2.5-fold (from 9 to 22 mol %), while that of 22:6 FA robustly increased approximately 7-fold (from 2 to 13 mol %) (Figure 5A). Intriguingly, the averaged changes of these four fatty acyl chains were 11.6 ± 2.7, 16.5 ± 3.2, 41.5 ± 7.5, and 58.2 ± 14.8% at days −2, 0, 7, and 14, respectively, relative to the levels of these FA chains at 7 days before birth. These changes were well-correlated with cell death in the developing cerebral cortex (i.e., 0.5, 0.9, 1.8, 3.3, 3.3, and 3.5% of TUNEL-positive nuclei at days −7, −5, −2, 0, 7, and 14, respectively) as previously reported (22).

Using enhanced shotgun lipidomics, we further determined the temporal course of alterations in the CL content in specific brain regions until advanced age (600 days) (Figures 4 and 5). We demonstrated that (1) the CL profile in mature murine neuronal tissue remained highly diversified throughout adult life, (2) this diversified CL profile was very different from that present during embryonic development, and (3) the content of signaling fatty acids (e.g., arachidonic and docosahexaenoic acids) remained relatively constant during adult life (Figures 4 and 5).

Changes in the mRNA Levels of Enzymes Involved in CL Synthesis and Remodeling Paralleled Age-Dependent Alterations in CL Composition

To identify the mechanisms underlying the diversification of the CL molecular profile in the developing mouse brain, we determined expression levels of mRNAs encoding selected enzymes involved in either CL *de novo* synthesis or remodeling by quantitative real-time PCR. These enzymes included CL synthase, phospholipases A_2, and tafazzin (i.e., a CL acyltransferase and/or transacylase). Real-time RT-PCR analyses demonstrated that the mRNA level of CL synthase was highest at 7 days before birth (the earliest day examined), dropped to a minimal level at day −2, fluctuated during the newborn period, and remained at a relatively low level at all later ages (inset of Figure 6A). The mRNA level of tafazzin was highest at day −7, gradually decreased to a minimum at day 20, and gradually increased from age 20 days to age 600 days at the end of the study (inset in Figure 6B). Because $iPLA_2$s have been previously demonstrated to be the predominant family of PLA_2 enzymes in the brain and may be involved in CL metabolism (35), we determined the mRNA levels of two of the major $iPLA_2$s (i.e., $iPLA_2\beta$ and $iPLA_2\gamma$). The expression levels of both enzymes were highest during prenatal development, with fluctuations during the newborn period and stabilization after 3 weeks of age (see insets in parts C and D of Figure 6). Therefore, the changes of the mRNA levels agreed well with the temporal changes in CL amount and molecular species composition, thereby identifying temporally coordinated alterations in neuronal CL content as well as molecular composition in perinatal murine CNS (see the Discussion).

Changes of the Expression Level of FACO Did Not Parallel the Temporal Changes in the Diversification of CL Profiles in Mouse Brain

It is well-established that glucose is the major fuel substrate used by the brain. During this study, we confirmed the lower rates of fatty acid β-oxidation of brain mitochondria in comparison to the heart as previously reported (31,36,37). It was found that the rate of fatty acid β-oxidation in mouse brain mitochondria was 3.0 ± 0.5 versus 160 ± 30 pmol min^{-1} (mg of protein)$^{-1}$ for mouse myocardial mitochondria. This result is consistent with the notion that a highly symmetric CL profile is associated with an efficient fatty acid β-oxidation. To verify whether the rate of fatty acid use for β-oxidation changed during the development of the brain and whether the oxidation rate difference is correlated with alterations in CL molecular species content and/or fatty acyl chain composition, we determined the temporal course of FACO mRNA expression levels by real-time RT-PCR analysis at the different stages of mouse brain development and aging. FACO mRNA levels increased dramatically during prenatal

development (peaking at birth and decreasing afterward; inset in Figure 7) and then declined gradually over the lifetime of the animal (Figure 7).

CL Molecular Species Profile Was Not Changed in Primary Neuronal Cultures under Varying Culture Conditions

We cultured neuronal cells from the neocortices of mice of 15−17 days gestation with a negligible amount of non-neuronal cells as described under the Materials and Methods. Shotgun lipidomics analyses demonstrated that the CL molecular profile was essentially identical to that found in the brain of prenatal mice (Figure 8). The diversified CL profile in the cultured neuronal cells was not changed with alterations in cell-culture conditions, such as glucose levels and bovine fetal serum content in the culture media as well as changes in cell-culture duration. Collectively, these results indicate that the perinatal diversification of CL in the brain likely does not result from alterations in the source of fuel used as substrate alone but rather represents an integral part of the chemical changes that occur in mitochondrial function and signaling in the perinatal period.

DISCUSSION

It has been recognized for many years that programmed cell death of neurons rapidly occurs in the perinatal period, leading to massive amounts of apoptosis and neuronal remodeling (23). Moreover, a regulatory element in the neuronal perinatal apoptotic program is the release of cytochrome *c* from the mitochondrial membrane, where it can activate caspase 3 and lead to programmed cell death (4–8). In the current study, using our recently developed enhanced shotgun lipidomics approach for CL analysis (10), we identified the massive remodeling of CL molecular species in the perinatal period and an increased number of the CL molecular species present in the developing brain. These alterations are highly correlated with the massive remodeling of neuronal circuitry that occurs in the developing cerebral cortex as previously reported (22).

We also unexpectedly demonstrated that CL molecular species in the brain contained a substantially more complex FA chain profile than that of any other previously examined tissues. We found that the content of fatty acids in CL molecular species in the cortex of mice at 4 months of age was 41, 24, 13, 9, 6, 4, and 1 mol % of 18:1, 20:4, 22:6, 18:2, 16:1, 16:0, and 18:0 FA, respectively, which differs dramatically from that of murine heart [i.e., 82, 7, 6, 2, and 2 mol % of 18:2, 22:6, 18:1, 20:3, and 20:2 FA, respectively (10)]. Therefore, it is possible that over 1000 different molecular species of CL could exist in the brain. In practice, at the current level of sensitivity, we demonstrated a total of over 50 isomeric ion peaks and identified over 100 CL molecular species. This number would likely increase dramatically after individual regioisomers resulting from the diastereotopic interactions introduced by the three glycerol molecules were determined. We found that the profile of CL molecular species varied from one brain region to another and also that variations exist between species. However, the marked diversity of CL molecular species was maintained in all brain regions in all species examined.

Multiple synthetic steps are involved in CL *de novo* synthesis. The rate-determining step in the *de novo* CL biosynthesis pathway is the reaction of CDP-diacylglycerol with glycerol-3-phosphate, which is mediated by phosphatidylglycerol phosphate synthase, to yield phosphatidylglycerol phosphate. Subsequent dephosphorylation (catalyzed by phosphatidylglycerol phosphate phosphatase activity) results in the generation of phosphatidylglycerol, a substrate for the final step in CL biosynthesis. Condensation of phosphatidylglycerol with CDP-diacylglycerol results in the generation of CL catalyzed by CL synthase. Therefore, the nascent CL carries the FA chains initially present in phosphatidylglycerol and phosphatidic acid. The nascent CL species are remodeled to yield

mature CL species by the sequential actions of phospholipases and re-acylation catalyzed by tafazzin or other transacylase or acyltransferase activities. Thus, the maturation of CL molecular species by remodeling represents a spatially and temporally coordinated mechanism for the biosynthesis of specific molecular species of CL that may be destined to perform specific physiological functions. Perinatal diversification of CL molecular species may occur either by (1) an increase in the *de novo* biosynthesis leading to enrichment in nascent CL molecular species, (2) an accelerated phospholipase activity and an increased re-acylation and a relative enrichment in the remodeled molecular species, or (3) combinations of these phenomena. In the present case, it seems likely that coordinated transcriptional programs are operative, leading to the dramatic changes in CL facilitating the remarkable neuronal plasticity present in the neonatal brain. Quantitative real-time RT-PCR analyses of mRNA expression demonstrated minimal alterations in CL synthase mRNA levels after the newborn period. In contrast, the mRNA expression levels of tafazzin as well as iPLA$_2\beta$ and iPLA$_2\gamma$ [both of which have been found in mitochondria previously (38–40)] are higher than that of CL synthase, and remodeling is much faster than *de novo* synthesis in cases where it has been carefully examined. This is likely the case in the perinatal brain, where the abundance of 18:1 CoA (41–43) and 18:1-containing phospholipids (25,34) for CL remodeling through acyltransferase activities and transacylation, respectively, would seem to be favored. Particularly, the level of tafazzin mRNA is relatively higher during the aging process compared to newborn levels, suggesting its role in the aging process. It is noteworthy that the enzymes that are involved in both the biosynthesis and remodeling of CL are abundantly expressed during the embryonic period, corresponding to a significant increase in the content of CL during brain development. The CL content, the FA chain composition of the CL pool, and the mRNA levels of CL metabolizing enzymes undergo rapid changes during the perinatal development of the brain (between days −7 and 12) (Figures 4 and 5). FA chains comprised of 16:1 and 18:1 moieties represent newly synthesized CL from phosphatidic acid and phosphatidylglycerol precursors (25,34) that are predominant during this period (Figure 5). Substantial increases in the levels of 20:4 and 22:6 FA (approximately 3- and 6-fold, respectively) occur from days −7 to 30 in CL and are indicative of a dramatic remodeling of CL into the mature species. Accordingly, both the lipidomics and real-time PCR analyses of enzymes involved in CL synthesis and remodeling are consistent with the notion that perinatal remodeling of CL likely participates in the coordinated development of the adult brain. The possibility that these alterations may reflect alterations in the dietary composition and absorption in the newborn period can not be ruled out but seems unlikely to be predominantly responsible because other tissues do not undergo similar amounts of perinatal remodeling after birth. The remarkable increases in total CL content in the newborn period indicates the presence of significant mitochondrial biogenesis, which is consistent with the increased speed of mitochondrial motility as well as the increased population of mitochondria at the dendritic spines during the early developmental stages (44–46).

The fact that the majority of cell types possess a CL profile containing predominantly one fatty acid to ensure the presence of a pool of largely symmetrical CL molecular species has been well-documented (9,10,47). The relationship of such a highly symmetrical CL profile with effective mitochondrial function has also been validated through the identification of the genetic basis of Barth syndrome (14,47). Genetic mutations in the X-linked gene, tafazzin, in Barth syndrome induce an altered CL metabolism, precipitate mitochondrial dysfunction, and affect multiple systems of the body, including changes to metabolism, motor delays, hypotonia, delayed growth, cardiomyopathy, weakened immune system function, chronic fatigue, hypoglycemia, mouth ulcers, diarrhea, and varying degrees of physical and mental disabilities (14). In the current study, we identified the substantial remodeling of CL molecular species and an increased amount of CL molecular species in the neonatal brain during perinatal development that occurred concomitantly with massive amounts of programmed neuronal death.

Intriguingly, a diversified CL profile is also present in the mature brain, although the degree of the diversity is less than that present immediately following postnatal neuronal remodeling. On the basis of prior results, the diversity and asymmetry present in the profile of brain CL molecular species is likely to reduce mitochondrial bioenergetic efficiency through suboptimal interactions with components of the electron-transport chain (7). This rationale has been supported through the demonstration of lower brain mitochondrial function in comparison to those of the heart and liver, including carnitine acyltransferase activities, respiratory rates, fatty acyl-CoA oxidation, among others (36,48–50). Why do brain mitochondria possess this highly diversified profile of CL molecular species? One likely explanation is that the brain relies predominantly on glucose as its major source of energy (in contrast to other organs) and that the rate of respiration is not a limiting factor in neuronal function. Thus, it seems likely that the roles of altered CL distribution are related to alterations in neuronal cellular signaling. The low rate of fatty acid oxidation by brain mitochondria in comparison to that of mitochondria from other organs supports this hypothesis. Surprisingly, primary neuronal cultures did not exhibit a similar diverse CL molecular profile during subculturing, growth, and maturation despite providing the cells with glucose as the major fuel substrate. These results indicate that the diversified CL profile present in the brain is likely associated with the regional (neuronal network) and/or global brain function.

On the basis of the present results, it seems likely that the perinatal alterations in CL in brain serve initially to determine neuronal cell fate during perinatal apoptosis. Subsequently, the diversity of CL molecular species in the adult brain facilitate cellular signaling and metabolic adaptation through interactions with cytochrome *c*, electron-transport proteins, and ion channels, as well as other mitochondrial proteins. Finally, the high content of signaling fatty acids (e.g., arachidonic acid and docosahexaenoic acid) in CL molecular species present in adult murine brain could serve as a reservoir for lipid second messenger generation by phospholipases acting upon CL. When the unique molecular geometry and physical properties of individual molecular species of CL in the brain are exploited, specific stereoelectronic interactions between CL and resident mitochondrial proteins can result in multiple additional avenues through which mitochondria can both regulate as well as energize neuronal cells.

REFERENCES

1. Schlame M, Rua D, Greenberg ML. The biosynthesis and functional role of cardiolipin. Prog. Lipid Res 2000;39:257–288. [PubMed: 10799718]
2. Hoch FL. Cardiolipins and biomembrane function. Biochim. Biophys. Acta 1992;1113:71–133. [PubMed: 1550861]
3. Hatch GM. Cell biology of cardiac mitochondrial phospholipids. Biochem. Cell Biol 2004;82:99–112. [PubMed: 15052331]
4. Petrosillo G, Ruggiero FM, Paradies G. Role of reactive oxygen species and cardiolipin in the release of cytochrome *c* from mitochondria. FASEB J 2003;17:2202–2208. [PubMed: 14656982]
5. Iverson SL, Orrenius S. The cardiolipin—cytochrome *c* interaction and the mitochondrial regulation of apoptosis. Arch. Biochem. Biophys 2004;423:37–46. [PubMed: 14989263]
6. Gonzalvez F, Gottlieb E. Cardiolipin: Setting the beat of apoptosis. Apoptosis 2007;12:877–885. [PubMed: 17294083]
7. Chicco AJ, Sparagna GC. Role of cardiolipin alterations in mitochondrial dysfunction and disease. Am. J. Physiol. Cell Physiol 2007;292:C33–C44. [PubMed: 16899548]
8. Kagan VE, Tyurina YY, Bayir H, Chu CT, Kapralov AA, Vlasova BNA II, Tyurin VA, Amoscato A, Epperly M, Greenberger J, Dekosky S, Shvedova AA, Jiang J. The “pro-apoptotic genies” get out of mitochondria: Oxidative lipidomics and redox activity of cytochrome *c*/cardiolipin complexes. Chem.-Biol. Interact 2006;163:15–28. [PubMed: 16797512]
9. Schlame M, Ren M, Xu Y, Greenberg ML, Haller I. Molecular symmetry in mitochondrial cardiolipins. Chem. Phys. Lipids 2005;138:38–49. [PubMed: 16226238]

10. Han X, Yang K, Yang J, Cheng H, Gross RW. Shotgun lipidomics of cardiolipin molecular species in lipid extracts of biological samples. J. Lipid Res 2006;47:864–879. [PubMed: 16449763]
11. Li G, Chen S, Thompson MN, Greenberg ML. New insights into the regulation of cardiolipin biosynthesis in yeast: Implications for Barth syndrome. Biochim. Biophys. Acta 2007;1771:432–441. [PubMed: 16904369]
12. Hauff KD, Hatch GM. Cardiolipin metabolism and Barth syndrome. Prog. Lipid Res 2006;45:91–101. [PubMed: 16442164]
13. Schlame M, Ren M. Barth syndrome, a human disorder of cardiolipin metabolism. FEBS Lett 2006;580:5450–5455. [PubMed: 16973164]
14. Barth PG, Valianpour F, Bowen VM, Lam J, Duran M, Vaz FM, Wanders RJ. X-linked cardioskeletal myopathy and neutropenia (Barth syndrome): An update. Am. J. Med. Genet. A 2004;126:349–354. [PubMed: 15098233]
15. Gu Z, Valianpour F, Chen S, Vaz FM, Hakkaart GA, Wanders RJ, Greenberg ML. Aberrant cardiolipin metabolism in the yeast taz1 mutant: A model for Barth syndrome. Mol. Microbiol 2004;51:149–158. [PubMed: 14651618]
16. Sparagna GC, Johnson CA, McCune SA, Moore RL, Murphy RC. Quantitation of cardiolipin molecular species in spontaneously hypertensive heart failure rats using electrospray ionization mass spectrometry. J. Lipid Res 2005;46:1196–1204. [PubMed: 15772420]
17. Sparagna GC, Chicco AJ, Murphy RC, Bristow MR, Johnson CA, Rees ML, Maxey ML, McCune SA, Moore RL. Loss of cardiac tetralinoleoyl cardiolipin in human and experimental heart failure. J. Lipid Res 2007;48:1559–1570. [PubMed: 17426348]
18. Ellis CE, Murphy EJ, Mitchell DC, Golovko MY, Scaglia F, Barcelo-Coblijn GC, Nussbaum RL. Mitochondrial lipid abnormality and electron transport chain impairment in mice lacking α-synuclein. Mol. Cell. Biol 2005;25:10190–10201. [PubMed: 16260631]
19. Bayir H, Tyurin VA, Tyurina YY, Viner R, Ritov V, Amoscato AA, Zhao Q, Zhang XJ, Janesko-Feldman KL, Alexander H, Basova LV, Clark RS, Kochanek PM, Kagan VE. Selective early cardiolipin peroxidation after traumatic brain injury: An oxidative lipidomics analysis. Ann. Neurol 2007;62:154–169. [PubMed: 17685468]
20. Han X, Yang J, Yang K, Zhao Z, Abendschein DR, Gross RW. Alterations in myocardial cardiolipin content and composition occur at the very earliest stages of diabetes: A shotgun lipidomics study. Biochemistry 2007;46:6417–6428. [PubMed: 17487985]
21. Su X, Han X, Mancuso DJ, Abendschein DR, Gross RW. Accumulation of long-chain acylcarnitine and 3-hydroxy acylcarnitine molecular species in diabetic myocardium: Identification of alterations in mitochondrial fatty acid processing in diabetic myocardium by shotgun lipidomics. Biochemistry 2005;44:5234–5245. [PubMed: 15794660]
22. Thomaidou D, Mione MC, Cavanagh JF, Parnavelas JG. Apoptosis and its relation to the cell cycle in the developing cerebral cortex. J. Neurosci 1997;17:1075–1085. [PubMed: 8994062]
23. Roth KA, D'Sa C. Apoptosis and brain development. Ment. Retard. Dev. Disabil. Res. Rev 2001;7:261–266. [PubMed: 11754520]
24. Bligh EG, Dyer WJ. A rapid method of total lipid extraction and purification. Can. J. Biochem. Physiol 1959;37:911–917. [PubMed: 13671378]
25. Cheng H, Jiang X, Han X. Alterations in lipid homeostasis of mouse dorsal root ganglia induced by apolipoprotein E deficiency: A shotgun lipidomics study. J. Neurochem 2007;101:57–76. [PubMed: 17241120]
26. Zeng Y, Cheng H, Jiang X, Han X. Endosomes and lysosomes play distinct roles in sulfatide-induced neuroblastoma apoptosis: Potential mechanisms contributing to abnormal sulfatide metabolism in related neuronal diseases. Biochem. J 2008;410:81–92. [PubMed: 17939778]
27. Lin Z, Ahmad MU, Ali SM, Ahmad I. An efficient and novel method for the synthesis of cardiolipin and its analogs. Lipids 2004;39:285–290. [PubMed: 15233408]
28. Valianpour F, Mitsakos V, Schlemmer D, Towbin JA, Taylor JM, Ekert PG, Thorburn DR, Munnich A, Wanders RJ, Barth PG, Vaz FM. Monolysocardiolipins accumulate in Barth syndrome but do not lead to enhanced apoptosis. J. Lipid Res 2005;46:1182–1195. [PubMed: 15805542]

29. Hoppel CL, Kerner J, Turkaly P, Turkaly J, Tandler B. The malonyl-CoA-sensitive form of carnitine palmitoyltransferase is not localized exclusively in the outer membrane of rat liver mitochondria. J. Biol. Chem 1998;273:23495–23503. [PubMed: 9722587]
30. Rajapakse N, Shimizu K, Payne M, Busija D. Isolation and characterization of intact mitochondria from neonatal rat brain. Brain Res. Protoc 2001;8:176–183.
31. Hulbert AJ, Turner N, Hinde J, Else P, Guderley H. How might you compare mitochondria from different tissues and different species? J. Comp. Physiol., B 2006;176:93–105. [PubMed: 16408229]
32. Bastie CC, Hajri T, Drover VA, Grimaldi PA, Abumrad NA. CD36 in myocytes channels fatty acids to a lipase-accessible triglyceride pool that is related to cell lipid and insulin responsiveness. Diabetes 2004;53:2209–2216. [PubMed: 15331529]
33. Han X, Yang J, Cheng H, Ye H, Gross RW. Towards fingerprinting cellular lipidomes directly from biological samples by two-dimensional electrospray ionization mass spectrometry. Anal. Biochem 2004;330:317–331. [PubMed: 15203339]
34. Han X, Holtzman DM, McKeel DW Jr. Plasmalogen deficiency in early Alzheimer's disease subjects and in animal models: Molecular characterization using electrospray ionization mass spectrometry. J. Neurochem 2001;77:1168–1180. [PubMed: 11359882]
35. Sun GY, Xu J, Jensen MD, Simonyi A. Phospholipase A2 in the central nervous system: Implications for neurodegenerative diseases. J. Lipid Res 2004;45:205–213. [PubMed: 14657205]
36. Bird MI, Munday LA, Saggerson ED, Clark JB. Carnitine acyltransferase activities in rat brain mitochondria. Bimodal distribution, kinetic constants, regulation by malonyl-CoA and developmental pattern. Biochem. J 1985;226:323–330. [PubMed: 3977877]
37. Czerniczyniec A, Bustamante J, Lores-Arnaiz S. Improvement of mouse brain mitochondrial function after deprenyl treatment. Neuroscience 2007;144:685–693. [PubMed: 17084986]
38. Gadd ME, Broekemeier KM, Crouser ED, Kumar J, Graff G, Pfeiffer DR. Mitochondrial iPLA2 activity modulates the release of cytochrome *c* from mitochondria and influences the permeability transition. J. Biol. Chem 2006;281:6931–6939. [PubMed: 16407316]
39. Mancuso DJ, Han X, Jenkins CM, Lehman JJ, Sambandam N, Sims HF, Yang J, Yan W, Yang K, Green K, Abendschein DR, Saffitz JE, Gross RW. Dramatic accumulation of triglycerides and precipitation of cardiac hemodynamic dysfunction during brief caloric restriction in transgenic myocardium expressing human calcium-independent phospholipase A2γ. J. Biol. Chem 2007;282:9216–9227. [PubMed: 17213206]
40. Mancuso DJ, Sims HF, Han X, Jenkins CM, Guan SP, Yang K, Moon SH, Pietka T, Abumrad NA, Schlesinger PH, Gross RW. Genetic ablation of calcium-independent phospholipase A2γ leads to alterations in mitochondrial lipid metabolism and function resulting in a deficient mitochondrial bioenergetic phenotype. J. Biol. Chem 2007;282:34611–34622. [PubMed: 17923475]
41. Rosendal J, Knudsen J. A fast and versatile method for extraction and quantitation of long-chain acyl-CoA esters from tissue: Content of individual long-chain acyl-CoA esters in various tissues from fed rat. Anal. Biochem 1992;207:63–67. [PubMed: 1489101]
42. Deutsch J, Grange E, Rapoport SI, Purdon AD. Isolation and quantitation of long-chain acyl-coenzyme A esters in brain tissue by solid-phase extraction. Anal. Biochem 1994;220:321–323. [PubMed: 7978274]
43. Golovko MY, Murphy EJ. An improved method for tissue long-chain acyl-CoA extraction and analysis. J. Lipid Res 2004;45:1777–1782. [PubMed: 15210839]
44. Li Z, Okamoto K, Hayashi Y, Sheng M. The importance of dendritic mitochondria in the morphogenesis and plasticity of spines and synapses. Cell 2004;119:873–887. [PubMed: 15607982]
45. Chang DT, Honick AS, Reynolds IJ. Mitochondrial trafficking to synapses in cultured primary cortical neurons. J. Neurosci 2006;26:7035–7045. [PubMed: 16807333]
46. Chang DT, Reynolds IJ. Differences in mitochondrial movement and morphology in young and mature primary cortical neurons in culture. Neuroscience 2006;141:727–736. [PubMed: 16797853]
47. Schlame M, Towbin JA, Heerdt PM, Jehle R, DiMauro S, Blanck TJ. Deficiency of tetralinoleoyl-cardiolipin in Barth syndrome. Ann. Neurol 2002;51:634–637. [PubMed: 12112112]
48. Katyare SS, Bangur CS, Howland JL. Is respiratory activity in the brain mitochondria responsive to thyroid hormone action?: A critical re-evaluation. Biochem. J 1994;302:857–860. [PubMed: 7945213]

49. Brewer GJ, Jones TT, Wallimann T, Schlattner U. Higher respiratory rates and improved creatine stimulation in brain mitochondria isolated with anti-oxidants. Mitochondrion 2004;4:49–57. [PubMed: 16120374]

50. Bustamante J, Czerniczyniec A, Lores-Arnaiz S. Brain nitric oxide synthases and mitochondrial function. Front. Biosci 2007;12:1034–1040. [PubMed: 17127358]

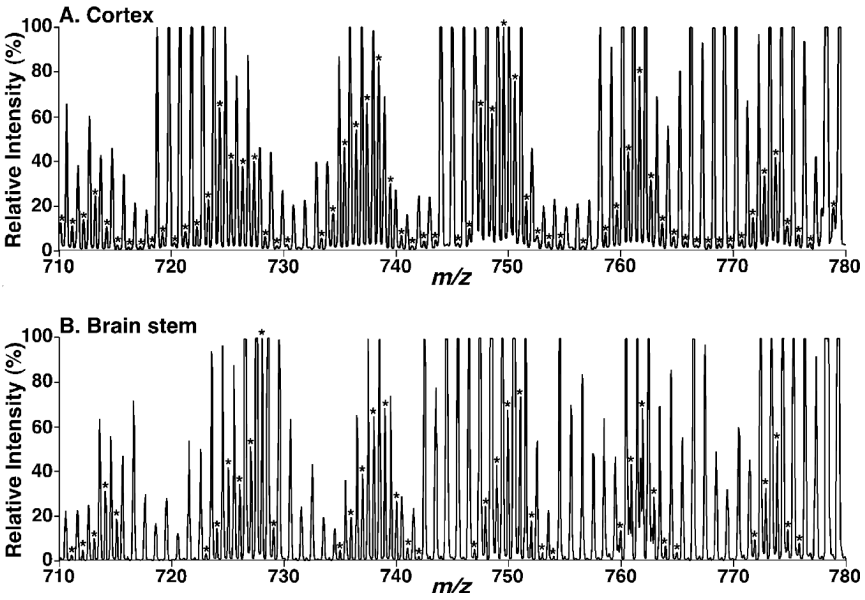

Figure 1.

Expanded negative-ion ESI mass spectra of mouse brain lipid extracts obtained using a QqTOF mass spectrometer. Lipid extracts of mouse cortex (A) and brain stem (B) were prepared by a modified Bligh and Dyer procedure, and electrospray ionization mass spectra were acquired in the negative-ion mode using a QqTOF mass spectrometer as described under the Materials and Methods. The asterisks indicate the identified CL plus-one isotopologues, which were characteristic of the doubly charged CL molecular species and were used to quantify individual CL molecular species based on ion intensity as previously described (10). Each spectrum is displayed after being normalized to the most abundant CL plus-one isotopologue.

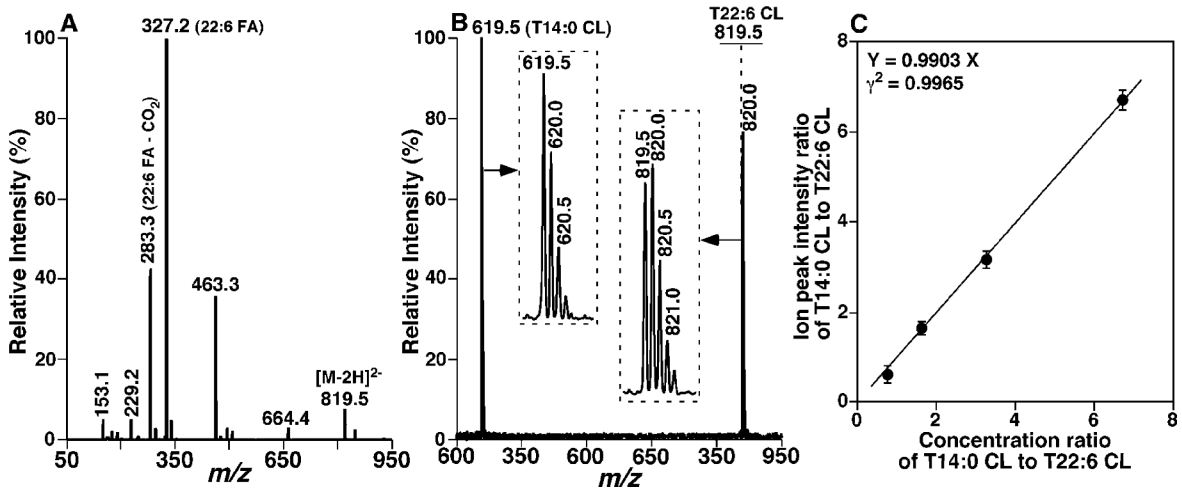

Figure 2.

Electrospray ionization mass spectrometric analyses of synthesized tetra22:6 cardiolipin. (A) Product ion mass spectrum of *m*/*z* 819.5, from which the selected ion can be identified as T22:6 CL. (B) Representative negative-ion ESI mass spectrum of an equimolar mixture of T14:0 CL and T22:6 CL (1 pmol/μL each). The insets display the isotopologue patterns of the ions. The horizontal line over the ion peak at *m*/*z* 819.5 represents the monoisotopic ion peak intensity after ^{13}C de-isotoping and has been normalized to that at *m*/*z* 619.5. (C) Linear correlation between the concentration ratios and the ion peak intensity ratios of T14:0 CL and T22:6 CL. The data points represent the mean ± SD determined at a variety of concentrations. These results indicate that the ionization response factors of T14:0 CL and T22:6 are essentially identical within experimental errors after ^{13}C de-isotoping.

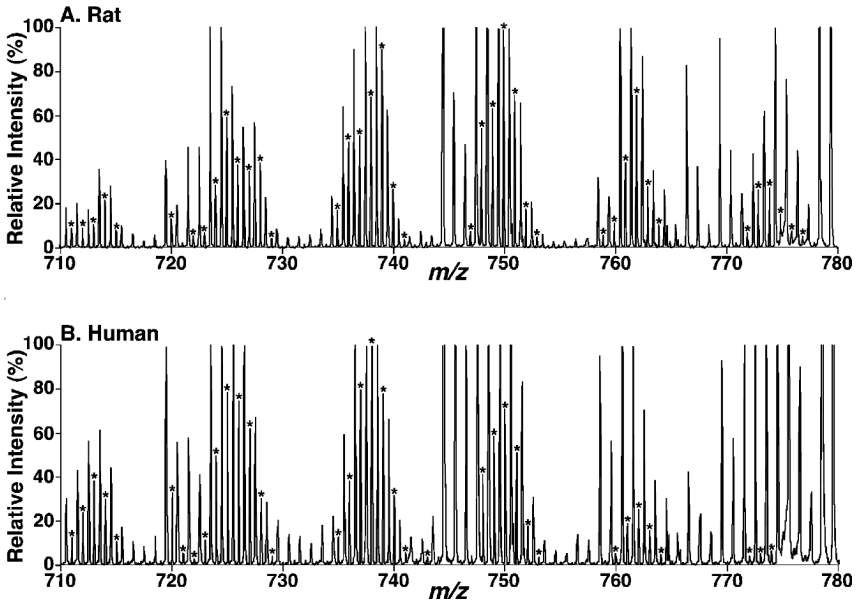

Figure 3.

Expanded representative negative-ion ESI mass spectra of lipid extracts of rat and human brain samples using a QqTOF mass spectrometer. Lipid extracts of rat cortex (A) and human cortex (B) were prepared by a modified Bligh and Dyer procedure, and electrospray ionization mass spectra were acquired in the negative-ion mode using a QqTOF mass spectrometer as described under the Materials and Methods. The asterisks indicate the identified CL plus-one isotopologues, which were characteristic of doubly charged CL molecular species and were used to quantify individual CL molecular species based on ion intensity as previously described (10). Each spectrum is displayed after being normalized to the most abundant CL plus-one isotopologue.

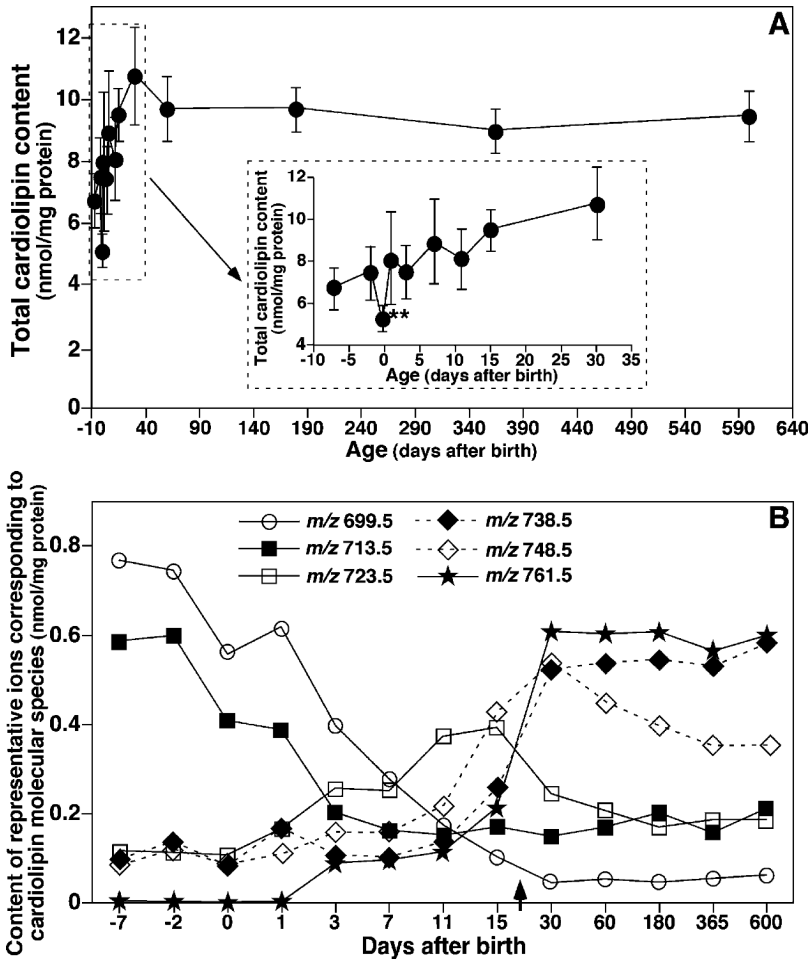

Figure 4.

Temporal changes in the contents of total CL and representative CL molecular species in lipid extracts of mouse cortex. Lipid extracts of mouse cortex at different ages before and after birth were prepared using a modified Bligh and Dyer method. The content of each individual CL molecular species after identification were calculated in comparison to the selected internal standard after ^{13}C de-isotoping as described under the Materials and Methods. (A) Temporal changes in the content of total CL, which was summarized from the determined contents of individual CL molecular species in mouse cortex before and after birth. The inset of A displays the region of the graph during the pre- and postnatal periods. (B) Temporal changes in the levels of multiple CL molecular species (as indicated and representative of the different mass regions) in lipid extracts of mouse cortex before and after birth. It should be noted that the scale of the *x* axis in B is random and represents the days when the animals were sacrificed after birth. Negative signs represent the number of days before birth. The data points represent mean ± SD from separate preparations of at least four different animals. The error bars in B are within the symbols. The arrow in B indicates the weaning time.

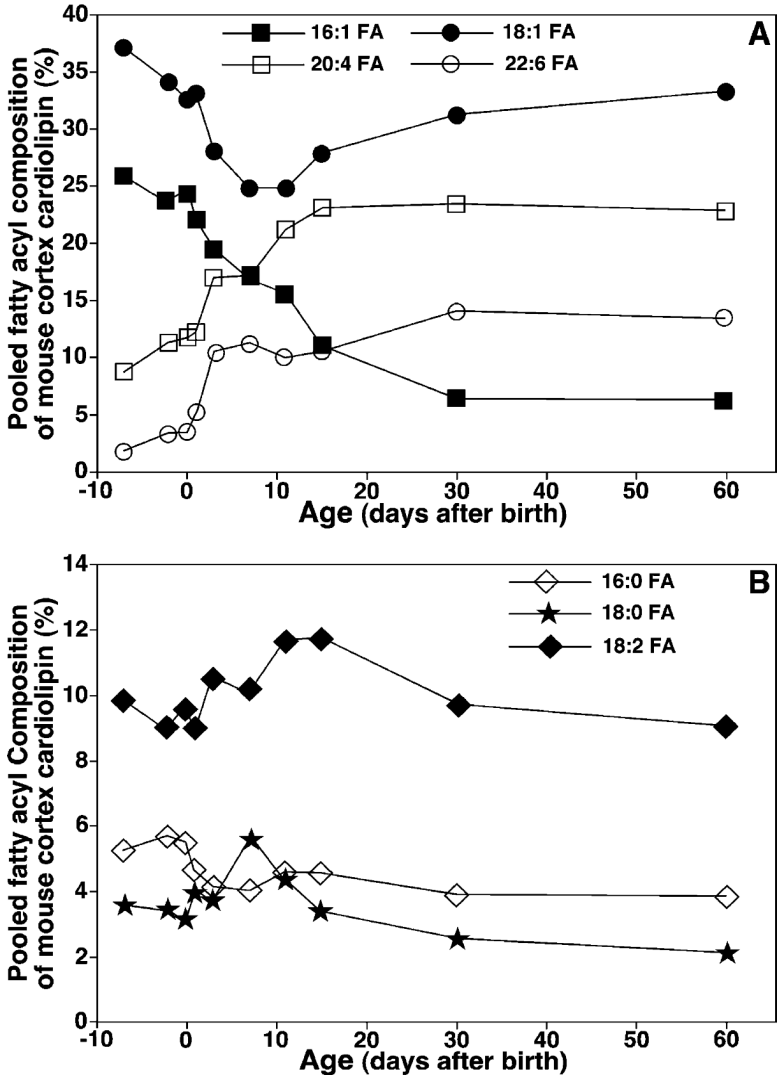

Figure 5.

Temporal changes of the FA composition of CL molecular species in mouse cortex before and after birth. The composition of the selected individual FA chains (as indicated) of the CL pool in mouse cortex were calculated from the determined averaged contents of individual CL molecular species as similarly described in the caption of Figure 4.

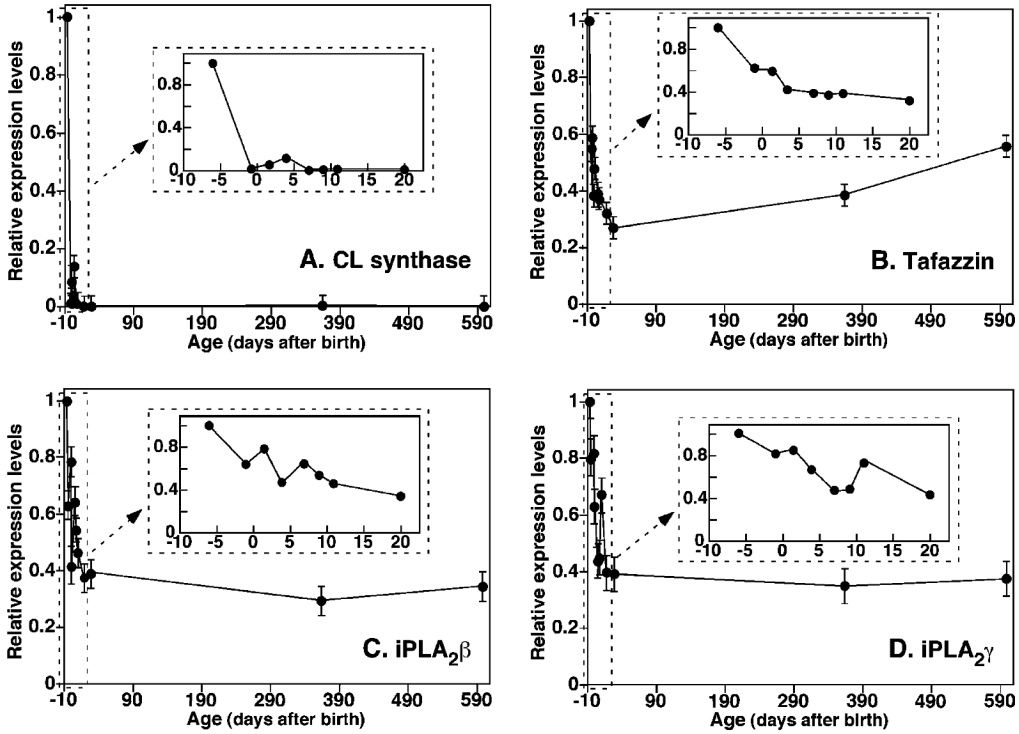

Figure 6.

Temporal changes of the relative mRNA levels of select CL biosynthetic and remodeling enzymes in mouse cortex before and after birth using quantitative real-time PCR analyses. Total RNA was isolated, and quantitative PCR was performed as described under the Materials and Methods. The forward and reverse primers as well as probes for CL synthase (A), tafazzin (B), calcium-independent phospholipase $A_2\beta$ (iPLA$_2\beta$) (C) and iPLA$_2\gamma$ (D) used in the analyses are listed under the Materials and Methods. Data represent the mean ± SD from separate preparations and analyses of at least three different animals. Data are expressed as normalized arbitrary units, with message levels normalized to that of mouse GAPDH, which was used as an internal control. The inset of each panel expands the pre- and postnatal time period.

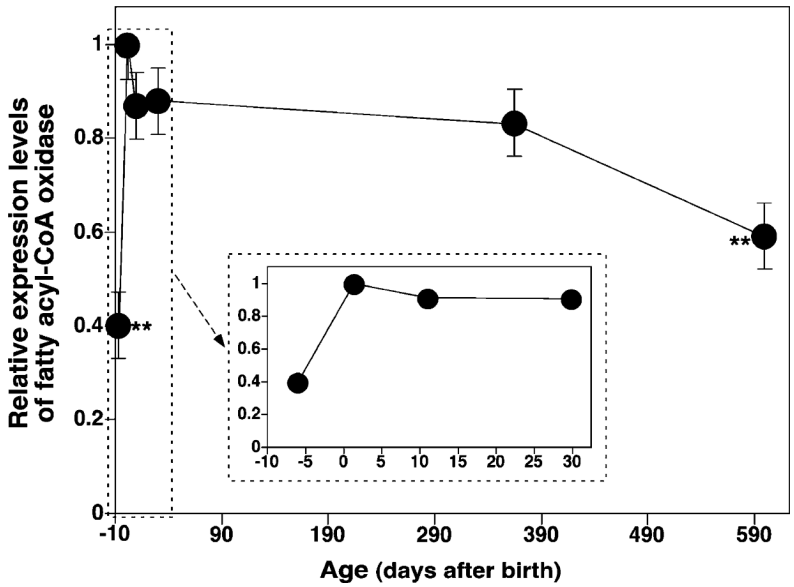

Figure 7.

Temporal changes of the relative mRNA levels of FACO in mouse cortex before and after birth using quantitative real-time RT-PCR analyses. Total RNA was isolated, and quantitative PCR was performed as described under the Materials and Methods. The forward and reverse primers as well as the probe for FACO used in the analyses were listed under the Materials and Methods. Data represent the mean ± SD from each of the separate preparations and analyses of at least three different animals. Data are expressed as normalized arbitrary units, with message levels normalized to that of mouse GAPDH, which was used as an internal control. The inset expands the region near the birth time.

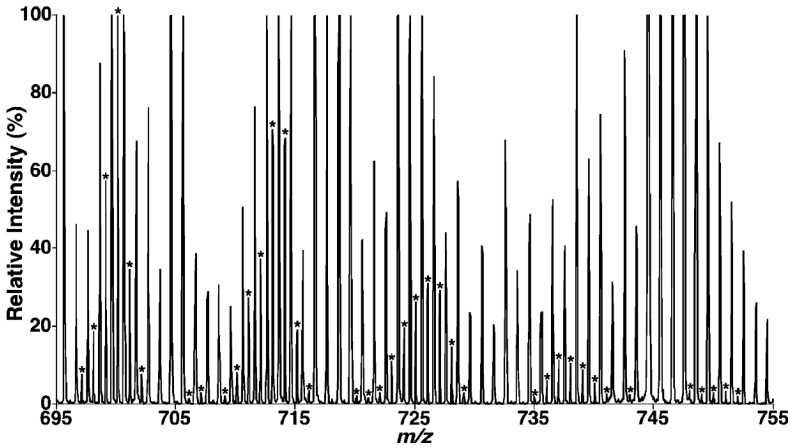

Figure 8.

Expanded negative-ion ESI mass spectrum of lipid extracts of primary neuronal cultures using a QqTOF mass spectrometer. Lipid extracts of cultured cells were prepared by a modified Bligh and Dyer procedure, and an ESI mass spectrum was acquired in the negative-ion mode using a QqTOF mass spectrometer as described under the Materials and Methods. The asterisks indicate the recognizable CL plus-one isotopologues, which were characteristic of doubly charged CL molecular species and were used to quantify individual CL molecular species based on ion intensity as previously described (10). The spectrum is displayed after being normalized to the most abundant CL plus-one isotopologue.

Table 1

Content of CL Molecular Species in Different Brain Regions of Mice at 4 Months of Age[a]

m/z	CL molecular species	cerebellum	cortex	spinal cord	brain stem
698.47	18:1−18:1−16:1−16:2 18:1−18:2−16:1−16:1	0.01 ± 0.00	0.01 ± 0.00	0.003 ± 0.001	0.02 ± 0.01
699.48	18:1−18:1−16:1−16:1	0.03 ± 0.01	0.03 ± 0.01	0.08 ± 0.01	0.05 ± 0.01
700.49	18:1−18:1−16:0−16:1 18:2−18:1−16:0−16:0 18:2−18:0−16:1−16:0	0.05 ± 0.01	0.03 ± 0.01	0.03 ± 0.02	0.08 ± 0.01
701.49	18:1−18:1−16:0−16:0 18:2−18:0−16:0−16:0 18:1−18:0−16:0−16:1	0.06 ± 0.01	0.02 ± 0.00	0.18 ± 0.01	0.09 ± 0.01
709.46	20:4−18:2−16:1−16:1	0.01 ± 0.00	0.003 ± 0.002	0.03 ± 0.01	0.01 ± 0.00
710.47	20:4−18:1−16:1−16:1 20:4−18:2−16:1−16:0	0.03 ± 0.00	0.05 ± 0.01	0.04 ± 0.00	0.04 ± 0.01
711.48	20:4−18:1−16:1−16:0 18:2−18:2−18:1−16:1	0.06 ± 0.01	0.06 ± 0.01	0.04 ± 0.00	0.07 ± 0.01
712.49	18:2−18:1−18:1−16:1 18:1−18:1−18:1−16:2 18:2−18:1−18:0−16:2 18:2−18:2−18:0−16:1	0.15 ± 0.02	0.10 ± 0.01	0.11 ± 0.01	0.15 ± 0.02
713.49	18:1−18:1−18:1−16:1 18:2−18:1−18:1−16:0	0.22 ± 0.03	0.15 ± 0.02	0.27 ± 0.01	0.42 ± 0.04
714.50	18:1−18:1−18:1−16:0 18:0−18:1−18:1−16:1	0.12 ± 0.02	0.05 ± 0.01	0.18 ± 0.01	0.24 ± 0.02
715.51	18:0−18:1−18:1−16:0 18:0−18:0−18:1−16:1	0.01 ± 0.00	0.003 ± 0.002	0.01 ± 0.00	0.003 ± 0.002
721.46	20:4−20:4−16:1−16:1	0.02 ± 0.00	0.03 ± 0.01	0.04 ± 0.01	0.03 ± 0.01
722.47	20:4−20:4−16:1−16:0 20:4−18:2−18:2−16:1	0.05 ± 0.01	0.06 ± 0.01	0.04 ± 0.00	0.06 ± 0.01
723.48	20:4−18:2−18:1−16:1	0.21 ± 0.03	0.36 ± 0.08	0.17 ± 0.03	0.24 ± 0.02
724.49	20:4−18:2−18:1−16:0 20:4−18:1−18:1−16:1	0.38 ± 0.04	0.49 ± 0.05	0.37 ± 0.02	0.66 ± 0.05
725.49	20:4−18:1−18:1−16:0 20:3−18:1−18:1−16:1 20:3−18:1−18:1−16:1	0.42 ± 0.05	0.34 ± 0.04	0.31 ± 0.03	0.51 ± 0.04
726.50	18:2−18:1−18:1−18:1	0.57 ± 0.08	0.35 ± 0.05	0.56 ± 0.02	0.81 ± 0.04
727.51	18:1−18:1−18:1−18:1	0.51 ± 0.06	0.28 ± 0.03	0.99 ± 0.05	1.44 ± 0.12
728.52	18:1−18:1−18:1−18:0	0.03 ± 0.01	0.003 ± 0.001	0.03 ± 0.02	0.06 ± 0.02
733.46	22:6−20:4−16:1−16:1	0.01 ± 0.01	0.01 ± 0.00	0.01 ± 0.01	0.02 ± 0.01
734.47	20:4−20:4−18:2−16:1	0.06 ± 0.00	0.10 ± 0.02	0.05 ± 0.01	0.08 ± 0.01
735.48	20:4−20:4−18:1−16:1	0.19 ± 0.00	0.31 ± 0.05	0.11 ± 0.01	0.29 ± 0.03
736.49	20:4−20:4−18:1−16:0 22:6−18:1−18:1−16:1 22:6−18:2−18:1−16:0	0.43 ± 0.05	0.45 ± 0.05	0.29 ± 0.03	0.59 ± 0.07
737.49	20:4−18:2−18:1−18:1 22:6−18:1−18:1−16:0	0.56 ± 0.07	0.57 ± 0.07	0.55 ± 0.05	0.94 ± 0.10
738.50	20:4−18:1−18:1−18:1	0.40 ± 0.05	0.59 ± 0.04	0.38 ± 0.03	0.92 ± 0.11
739.51	20:4−18:1−18:1−18:0 20:3−18:1−18:1−18:1	0.16 ± 0.03	0.11 ± 0.01	0.14 ± 0.01	0.28 ± 0.03
746.47	22:6−18:3−18:2−18:2	0.08 ± 0.01	0.04 ± 0.02	0.05 ± 0.02	0.10 ± 0.01
747.48	20:4−20:4−18:2−18:2 20:4−20:4−20:4−16:0 22:6−20:4−18:1−16:1 22:6−22:6−16:0−16:0 22:6−18:2−18:2−18:2	0.22 ± 0.01	0.39 ± 0.06	0.17 ± 0.01	0.39 ± 0.05

Biochemistry. Author manuscript; available in PMC 2008 August 12.

m/z	CL molecular species	cerebellum	cortex	spinal cord	brain stem
748.49	20:4−20:4−18:2−18:1	0.40 ± 0.03	0.56 ± 0.05	0.27 ± 0.02	0.65 ± 0.05
749.49	20:4−20:4−18:1−18:1	0.58 ± 0.06	0.74 ± 0.11	0.46 ± 0.01	0.97 ± 0.10
750.50	22:6−18:1−18:1−18:1	0.58 ± 0.06	0.55 ± 0.06	0.63 ± 0.02	1.02 ± 0.12
	20:4−20:3−18:1−18:1				
751.51	22:6−18:1−18:1−18:0	0.11 ± 0.03	0.06 ± 0.00	0.12 ± 0.02	0.15 ± 0.02
752.52	20:4−20:2−18:1−18:0	0.02 ± 0.01	0.003 ± 0.003	0.04 ± 0.01	0.03 ± 0.01
	20:4−20:1−18:1−18:1				
753.53	20:4−20:1−18:1−18:0	0.03 ± 0.01	0.01 ± 0.00	0.02 ± 0.02	0.04 ± 0.01
754.53	20:4−20:1−18:0−18:0	0.02 ± 0.01	0.003 ± 0.002	0.003 ± 0.002	0.02 ± 0.01
758.47	22:6−20:4−20:4−16:1	0.07 ± 0.02	0.02 ± 0.01	0.004 ± 0.002	0.08 ± 0.01
	22:6−22:6−18:2−16:1				
759.48	22:6−20:4−18:2−18:2	0.19 ± 0.01	0.14 ± 0.03	0.03 ± 0.02	0.23 ± 0.02
	22:6−20:4−20:4−16:0				
	22:6−22:6−18:1−16:1				
760.49	22:6−20:4−18:2−18:1	0.48 ± 0.02	0.40 ± 0.06	0.40 ± 0.06	0.68 ± 0.06
761.49	22:6−20:4−18:1−18:1	0.52 ± 0.02	0.64 ± 0.08	0.40 ± 0.02	0.93 ± 0.05
762.50	22:6−20:4−18:1−18:0	0.28 ± 0.03	0.18 ± 0.01	0.20 ± 0.02	0.32 ± 0.02
	22:6−20:3−18:1−18:1				
763.51	22:4−20:4−18:1−18:1	0.05 ± 0.01	0.02 ± 0.00	0.12 ± 0.02	0.07 ± 0.01
	22:6−20:3−18:1−18:0				
764.52	22:4−20:4−18:1−18:0	0.05 ± 0.01	0.01 ± 0.01	0.14 ± 0.04	0.06 ± 0.01
770.47	22:6−20:4−20:4−18:3	0.03 ± 0.02	0.004 ± 0.002	0.003 ± 0.002	0.08 ± 0.01
771.48	22:6−22:6−20:4−16:0	0.15 ± 0.02	0.12	0.27 ± 0.07	0.17 ± 0.01
	20:4−20:4−20:4−20:4				
	22:6−20:4−20:4−18:2				
	22:6−22:6−18:2−18:2				
772.49	22:6−20:4−20:4−18:1	0.42 ± 0.04	0.31	0.26 ± 0.05	0.54 ± 0.02
773.49	22:6−22:6−18:1−18:1	0.58 ± 0.02	0.36	0.53 ± 0.08	0.81 ± 0.07
	22:6−20:4−20:3−18:1				
774.50	16:0−20:3−22:5−22:5	0.12 ± 0.02	0.004 ± 0.002	0.04 ± 0.02	0.14 ± 0.01
	18:2−20:3−20:3−22:5				
	18:0−18:1−22:6−22:6				
	18:0−20:3−20:4−22:6				
775.51	18:0−18:0−22:6−22:6	0.05 ± 0.01	0.003 ± 0.002	0.11 ± 0.02	0.10 ± 0.02
776.52	18:0−18:0−22:5−22:6	0.02 ± 0.01	0.003 ± 0.001	0.04 ± 0.02	0.01 ± 0.01
777.53	18:0−18:0−22:5−22:5	0.003 ± 0.002	0.003 ± 0.002	0.09 ± 0.03	0.01 ± 0.01
783.48	22:6−22:6−20:4−18:2	0.11 ± 0.02	0.09 ± 0.01	0.15 ± 0.05	0.13 ± 0.01
784.49	22:6−22:6−20:4−18:1	0.28 ± 0.01	0.29 ± 0.05	0.004 ± 0.002	0.43 ± 0.06
785.49	22:6−22:6−20:4−18:0	0.18 ± 0.01	0.06 ± 0.01	0.003 ± 0.001	0.19 ± 0.02
	22:6−22:6−20:3−18:1				
795.48	20:4−20:4−22:6−22:6	0.05 ± 0.03	0.003 ± 0.001	0.003 ± 0.002	0.11 ± 0.02
796.49	22:6−22:6−22:6−18:1	0.27 ± 0.03	0.11 ± 0.05	0.20 ± 0.05	0.30 ± 0.02
	22:6−22:6−20:4−20:3				
797.49	20:4−20:3−22:6−22:5	0.03 ± 0.02	0.003 ± 0.001	0.003 ± 0.002	0.03 ± 0.02
	22:6−22:6−22:6−18:0				
	22:6−22:6−22:5−18:1				
	total	10.73 ± 0.97	9.66 ± 0.78	9.75 ± 0.51	16.90 ± 1.20
	16:0 FA	1.56 (3.6)	1.50 (3.8)	1.57 (4.0)	2.40 (3.6)
	16:1 FA	2.12 (4.9)	2.40 (6.2)	1.66 (4.3)	2.66 (3.9)
	16:2 FA	0.08 (0.2)	0.05 (0.1)	0.06 (0.2)	0.09 (0.1)
	18:0 FA	1.03 (2.4)	0.36 (0.9)	1.35 (3.5)	1.40 (2.1)
	18:1 FA	17.60 (41.0)	15.81 (40.9)	18.0 (46.1)	30.68 (45.4)
	18:2 FA	3.58 (8.3)	3.55 (9.2)	3.10 (8.0)	5.13 (7.6)
	18:3 FA	0.11 (0.3)	0.04 (0.1)	0.05 (0.1)	0.18 (0.3)
	20:1 FA	0.06 (0.2)	0.01 (0.04)	0.04 (0.1)	0.08 (0.1)
	20:2 FA	0.01 (0.1)	0.01 (0.1)	0.02 (0.1)	0.02 (0.1)

m/z	CL molecular species	cerebellum	cortex	spinal cord	brain stem
	20:3 FA	1.46 (3.4)	0.92 (2.4)	1.16 (3.0)	1.98 (2.9)
	20:4 FA	8.73 (20.3)	9.42 (24.4)	6.81 (17.5)	13.49 (20.0)
	22:4 FA	0.07 (0.2)	0.02 (0.1)	0.20 (0.5)	0.10 (0.1)
	22:5 FA	0.13 (0.3)	0.01 (0.01)	0.25 (0.6)	0.16 (0.2)
	22:6 FA	6.60 (15.4)	4.90 (12.7)	4.71 (12.1)	9.24 (13.7)
	total FA	42.92 (100)	38.64 (100)	39.00 (100)	67.60 (100)

[a]Lipid extracts from brain samples were prepared using a modified Bligh and Dyer procedure (24). The CL molecular species in the lipid extracts were identified by searching for plus-one isotopologues of doubly charged CL ions followed by product-ion analyses of these plus-one isotopologues, which were listed in the second column. The CL molecular mass listed in the first column was obtained from the QqTOF mass spectrometer. The doubly charged CL plus-one isotopologues were used to quantify individual CL molecular species as previously described (10,20). The results are expressed in nmol/mg of protein and represent $X \pm$ standard deviation (SD) from at least four different animals. The ion peaks of CL molecular species that constituted less than 0.003 nmol/mg of protein as determined by the QqTOF mass spectrometer have been omitted from the table. The FA chain content and composition (indicated in parentheses) were calculated from the content of identified CL molecular species.